


Cite this: *RSC Adv.*, 2020, **10**, 11755

Mixed Tb/Dy coordination ladders based on tetra(carboxymethyl)thiacalix[4]arene: a new avenue towards luminescent molecular nanomagnets[†]

A. S. Ovsyannikov, ^{*a} I. V. Khariushin, ^b S. E. Solovieva, ^a I. S. Antipin, ^b H. Komiya, ^c N. Maret, H. Tanaka, ^c H. Ohmagari, ^c M. Hasegawa, J. J. Zakrzewski, ^d S. Chorazy, N. Kyritsakas, ^e M. W. Hosseini and S. Ferlay ^{*e}

The macrocyclic ligand calix[4]arene (L1) and its sulphur-containing analogue thia[4]calixarene (L2) are promising precursors for functional molecular materials as they offer rational functionalization with various organic groups. Here, we present the first example of lanthanide-based coordination polymers built from the macrocyclic thiacalix[4]arene backbone bearing four carboxylic moieties, namely, ligand H₄L3. The combination of H₄L3 with the Tb³⁺ and Dy³⁺ cations led to the formation of 1D ladder-type coordination polymers with the formula [Ln^{III}HL3DMF₃]ⁿ·(DMF) (where DMF = dimethylformamide and Ln = Tb or Dy, denoted as HL3-Tb and HL3-Dy), which resulted from the coordination of the lanthanide cations with the partially deprotonated ligand HL3³⁻ that behaved as a T-shape connector. The coordination sphere around the metal was completed by the coordinated DMF solvent molecules. By combining both Tb³⁺ and Dy³⁺ cations, isostructural heterobimetallic solid solutions HL3-Tb_{1-x}Dy_x were also prepared. HL3-Tb and HL3-Dy showed visible light photoluminescence originating from the f-f electronic transitions of pale green emissive Tb³⁺ and pale yellow emissive Dy³⁺ with efficient sensitization by the functionalized thia[4]calixarene ligand HL3. In the HL3-Tb_{1-x}Dy_x solid solutions, the Tb/Dy ratio governed both the emission colour as well as the emission quantum yield, which reached even 28% at room temperature for HL3-Tb. Moreover, HL3-Dy exhibited a slow magnetic relaxation effect related to the magnetic anisotropy of the dodecahedral Dy³⁺ complexes, which were well isolated in the crystal lattice by expanded organic spacers.

Received 9th February 2020
Accepted 2nd March 2020

DOI: 10.1039/d0ra01263g
rsc.li/rsc-advances

Introduction

Coordination polymers (CPs),^{1,2} MOFs³ and molecular networks^{4,5} have molecular architectures that offer properties such as gas storage,^{6,7} catalysis,^{8,9} magnetism^{10,11} and luminescence.¹²⁻¹⁴ The

generation of such molecular species is based on the formation of coordination bonds between organic coordinating ligands and metal centres or complexes.¹⁵ A large number of coordination polymers that display different connectivity patterns have been generated using different types of polytopic ligands and metals.

Concerning the luminescence properties⁷ of CPs, special attention has been devoted to lanthanide-based CPs,¹⁶⁻¹⁸ owing to their outstanding photoluminescence originating from the triplet excited states of f-f transitions. Lanthanide-based CPs may find applications in luminescence sensing, light emission together with photonics,¹⁹⁻²¹ and as ligands presenting a strong antenna effect,²² allowing energy transfer from an organic ligand to the metal. The use of macrocyclic ligands for the formation of such assemblies has been documented;²³ however, most of the reports are mainly related to porphyrin-based lanthanide CPs.²⁴

Concerning the magnetic properties of lanthanide-based CPs, examples of molecular nanomagnets have been reported earlier.²⁵⁻²⁷ In addition, LnCPs may combine both SMM behaviour and tunable photoluminescence, as shown recently.²⁸⁻³⁰

^aArbuzov Institute of Organic and Physical Chemistry, FRC Kazan Scientific Center, Russian Academy of Sciences, Arbuzov str. 8, Kazan 420088, Russian Federation. E-mail: osaalex2007@rambler.ru

^bKazan Federal University, Kremlevskaya str. 18, Kazan 420008, Russian Federation

^cCollege of Science and Engineering, Aoyama Gakuin University, 5-10-1 Fuchinobe, Chuo-ku, Sagamihara, Kanagawa 252-5258, Japan

^dFaculty of Chemistry, Jagiellonian University, Gronostajowa 2, 30-387 Krakow, Poland

^eUniversité de Strasbourg, CNRS, CMC UMR 7140, F-67000 Strasbourg, France. E-mail: ferlay@unistra.fr

† Electronic supplementary information (ESI) available: Analysis using Shape program, measured cells for the solid solutions, EDS analysis for the solid solutions, excitation spectra, absolute luminescence quantum yields, decay profile analysis and details of magnetic measurements. CCDC 1898825 and 1898826. For ESI and crystallographic data in CIF or other electronic format see DOI: 10.1039/d0ra01263g



For building new CPs based on macrocycles, the use of calixarene derivatives presents a nice alternative. Calix[4]arenes^{31–33} are macrocyclic compounds composed of four phenolic moieties bridged by methylene groups as in the “classic” calix[4]arene, CA, L1 (Fig. 1), sulphur atoms in the case of thiocalix[4]arene, TCA, L2 (Fig. 1),³⁴ or hydroxyl or mercapto groups as in tetramercaptothiocalix[4]arene (TMTCA).^{35,36} These molecules can be easily modified by the functionalization of the upper and/or lower rims of the macrocyclic scaffold. They can adopt four different conformations (cone, partial cone, 1,2-alternate and 1,3-alternate), which make these compounds attractive precursors for designing molecular networks. The generation of coordination polymers with various dimensionalities using tetrasubstituted (tetramercapto)(thia)calix[4]arene derivatives that bear different coordinating sites is well documented.³⁷

By combining functionalized calix[6]arene bearing amide groups, calix[8]arene,^{38,39} unsubstituted calix[4]arene and thiocalix[4]arene derivatives in cone conformation^{40–43} with lanthanides salts or mixtures of 3d/4f^{44–51} different types of clusters have been obtained. Among them, the use of calixarenes bearing carboxylic coordinating sites, for which the lanthanides cations present great affinity, has been reported for the formation of isolated complexes.^{52,53}

It is important to note that, to date, only a few lanthanide-based coordination networks involving calixarene derivatives, which are mainly formed by the tetrasulfonate derivatives of (thia)calix[4]arenes in cone conformation,^{54–57} have been reported. To the best of our knowledge, no examples involving carboxylate derivatives or (thia)calix[4]arenes in 1,3-alternate conformation have been reported so far.

Several calixarene derivatives bearing carboxylic/ate coordinating groups have been described. Among them, the compound **H₄L3** has been used in the formation of coordination polymers with 3d metals, such as Co(II) or Mn(II), and ancillary ligands.^{58,59} An analogous ligand without the *tert*-butyl groups has been used for the formation of coordination polymers with Ag⁺, Ni²⁺, Co²⁺, and Zn²⁺ together with K⁺.^{60,61} TMTCA derivative-based coordination polymers using 3d metals have also been reported⁶² and shown to form hydrogen-bonded networks.⁶³

In this study, we report the structure of a series of isostructural new 1D lanthanide-based coordination networks,

derived from tetrasubstituted TCA in 1,3-alternate conformation bearing carboxylate moieties (**HL3**³⁻). A series of isostructural, homo and heterometallic lanthanide-based periodic architectures (Dy/Tb, because of the isostructurality of the related CPs) has been prepared. Mixing lanthanide cations in solid solution coordination networks can lead to the combination of two phosphorescent centres with large emission differences, which is a common strategy to gain self-referenced luminescence. Heteronuclear lanthanide Gd/Eu or La/Tb, Tb/Eu or Dy/Ln polymers are usually reported for the fine-tuning (colour and brightness) of the corresponding luminescence properties.^{64–66} Generally, the mixed Eu/Tb compounds allow energy transfer in the mixed coordination polymers due to the optimal energy match between the lanthanide cations.^{67–72} But tuneable emission can also arise when mixed Tb/Dy coordination compounds are used.⁷³

The ligand fluorescence and Dy³⁺ and Tb³⁺ phosphorescence were thoroughly studied in the solid-state in the corresponding (Dy/Tb) solid solutions. In addition, the magnetic properties of the anisotropic Dy³⁺ compound were investigated in detail.

Results and discussion

Synthesis and structural details

The synthesis of compound **H₄L3** was achieved following a previously reported procedure that involves a nucleophilic substitution reaction between TCA and ethyl bromoacetate in the presence of Cs₂CO₃ in acetone, followed by hydrolysis under basic conditions using LiOH in a THF/H₂O mixture.^{63,74,75} The combination of compound **H₄L3** with lanthanide(III) nitrate salts (Ln = Tb or Dy) under solvothermal conditions in DMF (see Experimental part) led to the formation of isostructural 1D coordination networks. The structural investigation of both single crystals of **HL3**-Ln (Ln = Dy and Tb) was carried out using X-ray diffraction. The formula derived from the crystallographic analysis was found to be [C₄₈H₅₃O₁₂S₄Ln(C₃H₇NO)₃]·(C₃H₇NO)·[Ln^{III}HL3DMF₃]·(DMF), Ln = Dy or Tb, as shown in Table 1. In the present CP, the ligand/metal ratio is 1/1.

The crystals were composed of **HL3**³⁻ in its tris-deprotonated form (see Table 2 for C–O distances), the trivalent Ln cation (Ln^{III}) and four DMF solvent molecules. The description of the structure in the solid-state is reported below only for **HL3**-Tb. The terbium atom was octacoordinated and surrounded by oxygen atoms. Two carboxylate moieties coordinated with the lanthanide in a bidentate mode and the third carboxylate presented a monodentate coordination mode. The 3 oxygen atoms belonging to three DMF molecules completed the coordination sphere of Tb (Fig. 2c). Using the SHAPE program,⁷⁶ the geometry around the Tb centres was found to be a deformed triangular dodecahedron, as shown in ESI.†

The crystal also contained a non-coordinated DMF molecule occupying the interstices between antiparallel 1D coordination networks without forming any specific interactions with them. The terbium atoms acted as T-shaped connectors, connecting three carboxylate groups belonging to three adjacent **HL3**³⁻ ligands, leading to a double chain ladder-like structure (Fig. 2a and b and schematically represented in d).

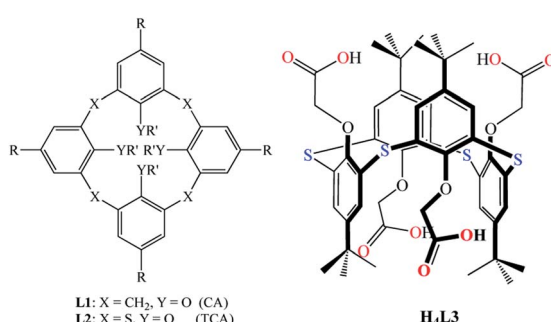


Fig. 1 Calix[4]arene (L1, CA) and thiocalix[4]arene (L2, CA) and tetramercaptothiocalix[4]arene derivative of thiocalix[4]arene (H₄L3) adopting a 1,3-alternate conformation.



Table 1 Crystallographic parameters for **HL3–Dy** and **HL3–Tb** recorded at 173 K

Formula	$C_{48}H_{53}O_{12}S_4Dy(C_3H_7NO)_3$, C_3H_7NO , $C_{60}H_{81}DyN_4O_{16}S_4$, HL3–Dy	$C_{48}H_{53}O_{12}S_4Tb(C_3H_7NO)_3$, C_3H_7NO , $C_{60}H_{81}TbN_4O_{16}S_4$, HL3–Tb
Molecular weight	1405.02	1401.44
Crystal system	Triclinic	Triclinic
Space group	$P\bar{1}$	$P\bar{1}$
a (Å)	15.0091(17)	15.0160(17)
b (Å)	15.9798(18)	15.9630(14)
c (Å)	16.7401(18)	16.7660(16)
α (deg)	62.217(5)	62.226(3)
β (deg)	67.626(5)	67.513(3)
γ (deg)	79.181(6)	79.132(4)
V (Å ³)	3284.5(7)	3285.2(6)
Z	2	2
Colour	Colourless	Colourless
Crystal dim (mm ³)	0.090 × 0.100 × 0.100	0.090 × 0.100 × 0.100
D_{calc} (g cm ⁻³)	1.421	1.417
$F(000)$	1454	1452
μ (mm ⁻¹)	1.332	1.270
Wavelength (Å)	0.71073	0.71073
Number of data meas	83 469	36 284
Number of data with $I > 2\sigma(I)$	17 032 [$R(\text{int}) = 0.0752$]	17 822 [$R(\text{int}) = 0.0558$]
R	$R_1 = 0.0557$, $wR_2 = 0.1391$	$R_1 = 0.0494$, $wR_2 = 0.1073$
R_w	$R_1 = 0.0756$, $wR_2 = 0.1559$	$R_1 = 0.0708$, $wR_2 = 0.1186$
GOF	1.057	1.011
Largest peak in final difference (eÅ ⁻³)	1.740 and -1.406	1.411 and -1.140

Consequently, the fourth carboxylic group remained protonated without interactions with the other components of the crystal.

As expected, different C–O distances were observed for the carboxylic moieties of **HL3**³⁻, revealing the presence of one non-coordinated carboxylic group and three coordinated carboxylate moieties (see Table 2).

Within the 1-D arrays, the shortest Tb–Tb distance was equal to 11.879(3) Å, and the packing of the 1D networks in the yOz plane (Fig. 2b, packing along the a -axis) led to a shorter Tb–Tb distance of 7.836(4) Å between two Tb atoms belonging to two different chains.

Since both compounds **HL3–Dy** and **HL3–Tb** were isostructural (which is not the case for Gd and Eu analogues, for example), solid solutions of formula **HL3–Tb_{1-x}Dy_x** were

prepared using the same synthetic procedure as the one used for **HL3–Dy** and **HL3–Tb** (see Experimental section). Meanwhile, in our case, the related Eu compound obtained with **H₄L3** was not isostructural with **HL3–Tb** or **HL3–Dy**.

Starting with different experimental Dy/Tb ratios, micro-crystalline compounds of the following formula were obtained: **HL3–Tb_{0.07}Dy_{0.93}**, **HL3–Tb_{0.20}Dy_{0.80}**, **HL3–Tb_{0.42}Dy_{0.58}**, **HL3–Tb_{0.67}Dy_{0.33}** and **HL3–Tb_{0.95}Dy_{0.05}**.

The structure of the solid solution was investigated by XRPD, as shown in Fig. 3 (for the determined cell parameters of the corresponding single crystals, see Table S1, ESI†). XRPD clearly demonstrated the structural homogeneity of the phase of the formed coordination compounds. All the **HL3–Tb_{1-x}Dy_x** solid

Table 2 Selected bond distances (Å) for **HL3–Dy** and **HL3–Tb**

	HL3–Dy	HL3–Tb
C–O (carboxyl-ate/-ic)	1.232(5) and 1.273(5) 1.239(5) and 1.268(4) 1.254(5) and 1.261(5) 1.189(5) and 1.323(5) (carboxylic)	1.215(4) and 1.269(4) 1.253(4) and 1.258(4) 1.243(4) and 1.259(4) 1.194(5) and 1.320(5) (carboxylic)
Ln–O (DMF)	2.354(3) 2.366(3) 2.380(3)	2.355(3) 2.369(2) 2.395(3)
Ln–O (carboxylate)	2.256(3) 2.380(3) 2.393(3) 2.404(3) 2.438(3)	2.277(2) 2.393(3) 2.411(3) 2.418(3) 2.440(2)



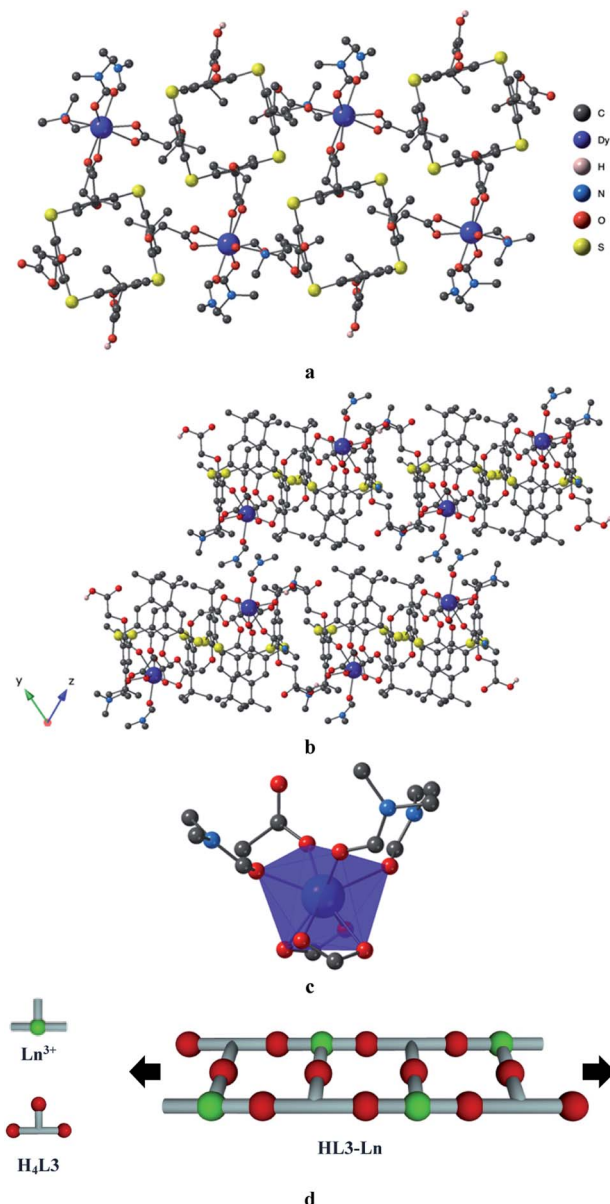


Fig. 2 (a) A portion of the crystal structure of **HL3-Tb**, (b) crystal packing of **HL3-Tb**, (c) the coordination environment of Ln^{3+} and (d) the schematic representation of connectivity in **HL3-Tb**.

solutions were isostructural and displayed the same structure as those of **HL3-Tb** or **HL3-Dy**. Since there was only one type of crystallographically independent Ln ion in the unit cell, owing to similar size of both lanthanide cations, one may assume a statistical distribution of the lanthanide cations in the crystal.

The composition of the $\text{HL3-Tb}_{1-x}\text{Dy}_x$ solid solutions was also checked using energy-dispersive X-ray spectroscopy (EDS), as shown in ESI†.

The experimentally determined Tb/Dy ratios measured were in good agreement with the relative quantities of the lanthanide salts used for synthesis. The slight differences were probably due to weighing inaccuracy and the overestimation of Tb^{3+} content in the EDS measurements (Table 3).

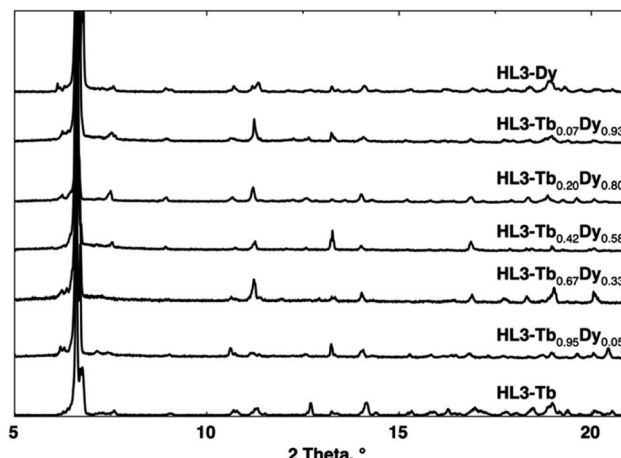


Fig. 3 Comparison of the simulated PXRD patterns for **HL3-Tb** (bottom) and **HL3-Dy** (top) and the recorded PXRD patterns for $\text{HL3-Tb}_{1-x}\text{Dy}_x$ solid solutions. Discrepancies in intensity between the observed and simulated patterns are due to the preferential orientations of the microcrystalline powders.

The luminescence and magnetic properties of this **HL3-Dy** series of compounds are presented below.

Photoluminescence properties

For all the investigated compounds, the measurements were carried out in the solid-state using polycrystalline powders.

Among the bands of the excitation spectra of **HL3-Tb** and **HL3-Dy** at RT in the 350–500 nm region with emission at $\lambda_{\text{em}} = 534$ nm and 576 nm, respectively (see Fig. S1, ESI†), those attributed to the typical f-f transitions of the Tb^{3+} and Dy^{3+} cations presented lower intensities compared with the band attributed to the $\pi \rightarrow \pi^*$ transitions of $\text{H}_4\text{L3}$ (300–350 nm). These observations clearly indicated the occurrence of an energy transfer from the excited level of ligand HL3^{3-} to the emitting state of the Tb^{3+} (or Dy^{3+}) cations, as seen in the case of antenna effect.⁷⁷ The capability of calixarene carboxylate derivatives to act as antennae for Tb^{3+} complexes has already been documented.⁵³

The room-temperature emission spectra of the **HL3-Tb** and **HL3-Dy** coordination networks, when excited at $\lambda_{\text{ex}} = 350$ nm, are depicted in Fig. 4. For **HL3-Tb**, the emission spectrum is composed of the characteristic five electronic transitions, *i.e.*, $^5\text{D}_4 \rightarrow ^7\text{F}_6$, $^5\text{D}_4 \rightarrow ^7\text{F}_5$ (strongest), $^5\text{D}_4 \rightarrow ^7\text{F}_4$, $^5\text{D}_4 \rightarrow ^7\text{F}_3$ and $^5\text{D}_4 \rightarrow ^7\text{F}_2$.

Table 3 Comparison of the observed and experimental Tb/Dy ratios in $\text{HL3-Tb}_{1-x}\text{Dy}_x$ coordination polymers

	Tb/Dy experimental ratio	Tb/Dy observed ratio (EDS)
HL3-Tb_{0.95}Dy_{0.05}	95 : 05	95 : 05
HL3-Tb_{0.67}Dy_{0.33}	60 : 40	67 : 33
HL3-Tb_{0.42}Dy_{0.58}	40 : 60	42 : 58
HL3-Tb_{0.20}Dy_{0.80}	20 : 80	20 : 80
HL3-Tb_{0.07}Dy_{0.93}	10 : 90	07 : 93



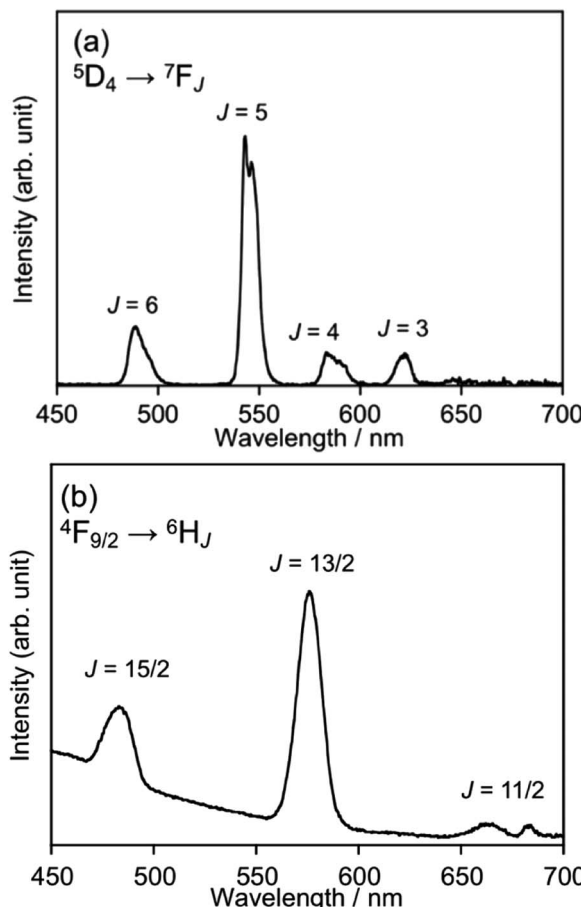


Fig. 4 Emission spectra ($\lambda_{\text{ex}} = 350$ nm) of **HL3-Tb** (a) and **HL3-Dy** (b) at RT.

$\rightarrow {}^7F_2$ (weakest), whereas for **HL3-Dy**, the ${}^4F_{9/2} \rightarrow {}^6H_{15/2}$, ${}^4F_{9/2} \rightarrow {}^6H_{13/2}$ (strongest) and ${}^4F_{9/2} \rightarrow {}^6H_{11/2}$ (weakest) electronic transitions are observed, as shown in Fig. 4a and b, respectively. These were typical f-f transitions with emission in the green region for Tb^{3+} and yellow-white region for Dy^{3+} . The corresponding emission spectra at 77 K are presented in Fig. S2a and b, ESI.[†]

The photophysical behaviour of the mixed $\text{HL3-Tb}_{1-x}\text{Dy}_x$ solid solutions was analysed at RT and 77 K. The luminescence spectra of the $\text{HL3-Tb}_{1-x}\text{Dy}_x$ solid solutions observed at RT and 77 K are shown in Fig. 5 and S3.[†]

At RT, the $\text{HL3-Tb}_{1-x}\text{Dy}_x$ solid solutions exhibited the typical luminescence bands of the f-f transitions of Tb^{3+} at 545 nm and those of Dy^{3+} at 574 nm. The band intensity at 545 nm decreased when x was decreased, and that at 574 nm increased when x was decreased, as shown in Fig. 5a and b. The introduction of Dy^{3+} in the $\text{HL3-Tb}_{1-x}\text{Dy}_x$ solid solutions allowed slight tuning of the emission colour ranging from pale green to pale yellow, as shown in Fig. 5a and b.

The absolute quantum yields of Tb^{3+} in the series of $\text{HL3-Tb}_{1-x}\text{Dy}_x$ solid solutions were observed (see Fig. S3a and b, ESI[†]), and the values at 77 K were found to be 58.9% (27.9% at RT) for **HL3-Tb**, 32.6% for $\text{HL3-Tb}_{0.95}\text{Dy}_{0.05}$, and 15.1% for

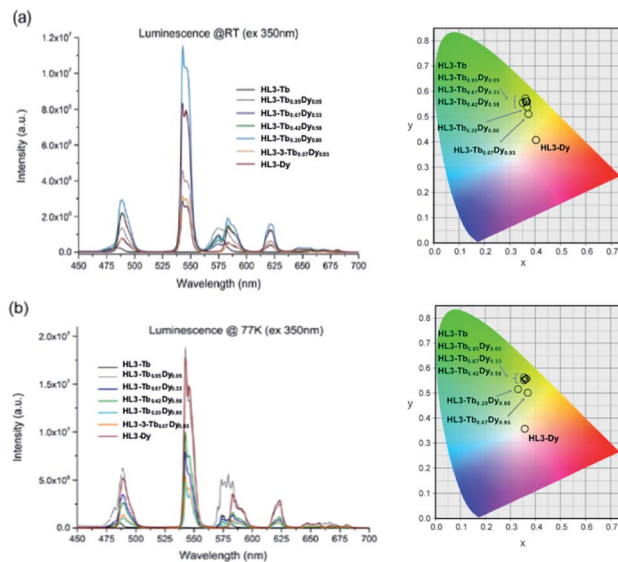


Fig. 5 Emission spectra ($\lambda_{\text{ex}} = 350$ nm) of **HL3-Dy** (black) and **HL3-Tb** (brown), and the solid solutions $\text{HL3-Tb}_{0.07}\text{Dy}_{0.93}$ (grey), $\text{HL3-Tb}_{0.20}\text{Dy}_{0.80}$ (blue), $\text{HL3-Tb}_{0.42}\text{Dy}_{0.58}$ (green), $\text{HL3-Tb}_{0.67}\text{Dy}_{0.33}$ (light blue) and $\text{HL3-Tb}_{0.95}\text{Dy}_{0.05}$ (orange) at (a) room temperature and (b) 77 K and the corresponding emission colours presented on the CIE 1931 chromaticity diagrams.

HL3-Tb. Therefore, the existence of Dy^{3+} ion in the solid solution played a role in decreasing the luminescence quantum yields of the $\text{HL3-Tb}_{1-x}\text{Dy}_x$ solid solutions.

The luminescence decay profile and fitted results are summarized in Tables S2 and S3 and Fig. S3–S5 in ESI.[†] As described above, the luminescence quantum yields of Dy^{3+} in the neat and solid solutions with Tb^{3+} were quite low, and it was not possible to obtain the decay profiles at both RT and 77 K for **HL3-Dy**. The lifetimes of **HL3-Tb** at RT and 77 K were estimated as a single component, and the τ values were 0.866 and 0.916 ms, respectively. After the addition of Dy^{3+} in the $\text{HL3-Tb}_{1-x}\text{Dy}_x$ solid solutions, the τ values decreased, and the number of luminescence components of Tb^{3+} increased to two or three (see Tables S2 and S3 in ESI[†]). The luminescence decay curve of $\text{HL3-Tb}_{0.2}\text{Dy}_{0.8}$ could be divided into two components, namely 0.378 and 0.932 ms ($\lambda = 543$ nm), at RT. The latter value corresponded to the one observed for **HL3-Tb**. The second and third emission lifetimes were related to the increasing number of Dy^{3+} centers surrounding the Tb^{3+} centers.

The τ_{obs} values (Tables S2 and S3 in ESI[†]) were in accordance with those reported for other calixarene-based coordination compounds in the solid-state.^{53,78}

Magnetic measurements

As **HL3-Dy** contains the magnetically anisotropic Dy^{3+} cations, which may lead to a potential single-molecule magnet character, its magnetic properties were investigated. The magnetic behaviour of **HL3-Tb** is not presented here because of the lack of significant anisotropy for Tb. As shown in Fig. 6, at 300 K, the $\chi_M T$ product reached $14.1 \text{ cm}^3 \text{ mol}^{-1} \text{ K}$, which is the exact value



expected for free-ion approximation. A typical decrease in the $\chi_M T$ product was observed upon cooling, which could be related to thermal depopulation within the m_j levels of the ground $^6H_{15/2}$ multiplet of Dy^{3+} . Besides a slow decrease in the signal, the $\chi_M T$ versus T plot did not display abrupt changes, which suggested the lack of magnetic interactions down to 1.8 K as a result of the efficient magnetic isolation of lanthanide centres in the crystal lattice. Magnetization measured at $T = 1.8$ K increased quickly with increasing magnetic field to 10 kOe and much slower at higher fields, reaching $5.4 \mu_B$ at 60 kOe without saturation, as expected for anisotropic Dy^{3+} (inset in Fig. 6).⁷⁹

To investigate the slow magnetic relaxation effects in **HL3-Dy**, the alternate-current (ac) magnetic characteristics were gathered at $H_{dc} = 0$ (Fig. 7a). The maxima of the frequency dependence of out-of-phase magnetic susceptibility, χ_M'' , appeared on the edge of the measurement range, even at 1.8 K, quickly moving towards higher frequencies while the temperature increased. This indicated the presence of slow magnetic relaxation, a characteristic effect of the single-molecule magnet (SMM) behaviour. To slow down the relaxation by reducing the presumably disturbing quantum tunnelling of the magnetization (QTM) process, an external dc magnetic field was applied (see Fig. S7, ESI†). The field-variable ac magnetic characteristics were analysed using the generalized Debye model for a single relaxation.⁸⁰ The extracted relaxation times were plotted against the magnetic field, and the resulting dependence was analysed by taking into account the QTM effect (Quantum Tunnelling of the Magnetisation), which was dominant at low fields, and a field-induced direct process responsible for the acceleration of the relaxation process at higher fields (see ESI, Fig. S7†).⁸¹ An equilibrium between these processes appeared at $H = 1000$ Oe, which was selected as the optimal dc field to investigate magnetic relaxation in **HL3-Dy**. The dc magnetic characteristics were gathered in the 1.8–5 K temperature range (Fig. 7b and see Fig. S8, ESI†). They were analysed using the generalized Debye model for a single relaxation, and the resulting relaxation times are presented as the function of temperature (Fig. 7c).

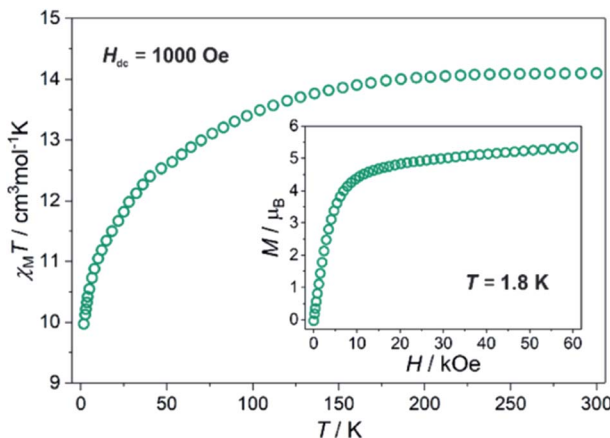


Fig. 6 The temperature dependence of the $\chi_M T$ product of **HL3-Dy** at $H_{dc} = 1000$ Oe, and the field dependence of molar magnetization at $T = 1.8$ K (inset).

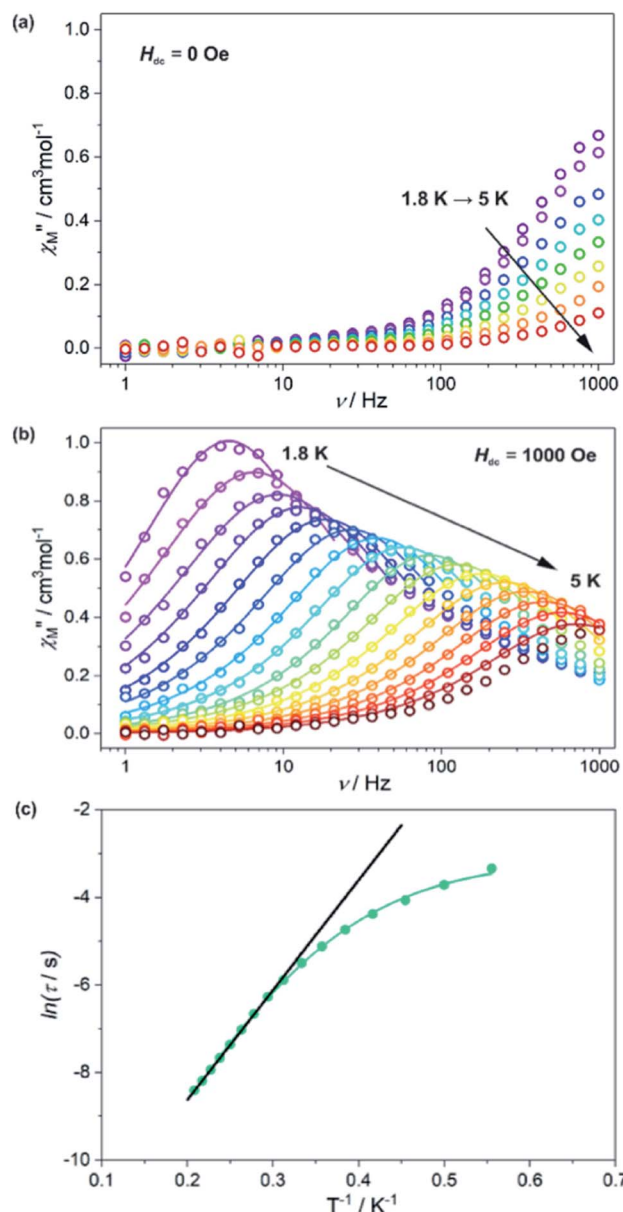


Fig. 7 For **HL3-Dy**: (a) Zero dc field $\chi_M''(\nu)$ curves in the range of 1.8–5 K, (b) dc field $\chi_M''(\nu)$ curves in the range 1.8–5 K under a dc field of 1 kOe, and (c) temperature dependence of the relaxation time, τ , at 1 kOe, fitted using the Arrhenius law in the limited 3.4–5 K range (extrapolated black line) and within the full 1.8–5 K range using the contributions from the Orbach, Raman, direct and QTM relaxation processes (green line; see text for details).

In the higher temperature range of 3.4–4.8 K, the temperature dependence of the relaxation times was close to linear, and thus, it could be analysed by a simple Arrhenius law, which is presented in eqn (1):

$$\ln(\tau) = \frac{U_{\text{eff}}}{k_B T} + \ln(\tau_0) \quad (1)$$

where U_{eff} represents the effective thermal energy barrier, while τ_0 is the relaxation attempt time for spin reversal at infinite temperature. The obtained parameters $U_{\text{eff}}/k_B = 25.08(9)$ K, $\tau_0 =$



$1.2(2) \times 10^{-6}$ s were within the characteristic limits of single-molecule magnets with moderate magnetic anisotropy.⁷⁹ More precisely, the full temperature dependence curve of the relaxation times was fitted using contributions from the Orbach and Raman relaxation processes together with direct and QTM processes taken from the previous analysis of field-dependent relaxation. Therefore, eqn (2) was used:

$$\tau^{-1} = \tau_1^{-1} \exp(-U_{\text{eff}}/k_B T) + B_{\text{Raman}} T^n + \frac{a(1+c^2 H^2)}{(1+bH^2)} + A TH^4 \quad (2)$$

where the first term represents the Orbach process related to the Arrhenius law, the second introduces a two-phonon Raman relaxation pathway, the third denotes the QTM effect and the last one shows a direct process.^{82,83} To avoid over-parameterization, the two last terms describing the QTM effect and direct process taken from the field-dependence analysis and the related parameters were not optimized during the fitting procedure (Fig. S8†). The obtained values $U_{\text{eff}}/k_B = 31(3)$ K and $\tau_0 = 1.2(7) \times 10^{-6}$ s were in good agreement with those extracted from the Arrhenius law. The Raman process had to be included with $B_{\text{Raman}} = 0.27(1) \text{ s}^{-1} \text{ K}^{-n}$ and $n = 6.0(3)$. Thus, the last value expected for lanthanide-based SMMs would be located in the 2–9 range.³⁹ As several examples of SMMs lacking the Orbach process have been reported,⁸⁴ we tried to fit the temperature dependence of the relaxation times excluding Orbach process; however, it was not possible to obtain a satisfying fit.

Based on these results, we could clearly postulate that the Dy^{3+} complexes in **HL3-Dy** exhibit single-molecule magnet characteristics with a moderated thermal energy barrier originating from the Orbach relaxation process and a strong QTM effect, partially reduced by using the external dc magnetic field.

Conclusions

In this work, we have demonstrated the possibility of growing a series of lanthanide-based isostructural homometallic coordination polymers using thiocalix[4]arene bearing carboxylic moieties. Owing to their isostructural nature, a series of unprecedented heterometallic solid solutions based on the macrocyclic thiocalix[4]arene derivatives were generated. The single crystals of the two isostructural Tb^{3+} - and Dy^{3+} -based coordination polymers (**HL3-Tb** and **HL3-Dy**, formula $[\text{Ln}^{III}\text{HL3DMF}_3]\cdot(\text{DMF})$) were structurally characterized using X-ray diffraction, and their photophysical properties were investigated. The formation of the 1D ladder-type coordination compounds resulted in the specific binding of the Ln^{3+} cation to the partially deprotonated organic ligands that behaved as a “T-Shape” connector. In the solid solutions that combined Tb^{3+} and Dy^{3+} forming $\text{HL3-Tb}_{1-x}\text{Dy}_x$, the Ln^{3+} cations are randomly distributed within the crystals.

The photoluminescence properties of the coordination polymers were investigated. Ligand **HL3**³⁺ sensitized the luminescence of the Tb^{3+} or Dy^{3+} cations in **HL3-Tb** and **HL3-Dy** at RT, and they exhibited the characteristic f-f transition due to the presence of the Ln^{3+} cations. The introduction of Dy^{3+} in

HL3-Tb allowed the tuning of the emission colour of the solid solutions, which ranged between pale yellow and pale green.

In addition, the magnetic measurements of **HL3-Dy** revealed significant magnetic anisotropy in the Dy^{3+} complexes attached to the thiocalix[4]arene moieties, leading to SMM behaviour. Therefore, this series of new coordination polymers can be considered as a novel source of bifunctional magnetoluminescent molecule-based materials.⁸⁵ We present a novel and elegant pathway for the construction of luminescent molecular nanomagnets by the incorporation of lanthanide ions in coordination chains based on functionalized thiocalix[4]arene ligands.

Experimental methods

X-ray crystallography

Data were collected at 173(2) K on a Bruker Apex-II-CCD diffractometer equipped with an Oxford Cryosystem liquid N_2 device using graphite-monochromated Mo-K α ($\lambda = 0.71073 \text{ \AA}$) radiation. For all the structures, diffraction data were corrected for absorption. The structures were solved using SHELXS-97 and refined by full matrix least-squares on F^2 using SHELXL-97. Hydrogen atoms were introduced at calculated positions and refined using a riding model.⁸⁶ The structures can be obtained free-of-charge from the Cambridge Crystallographic Data Centre via www.ccdc.cam.ac.uk/datarequest/cif. CCDC: 1898825 (**HL3-Tb**) and 1898826 (**HL3-Dy**).

Powder diffraction studies (PXRD)

The diffraction diagrams were collected on a Bruker D8 diffractometer using monochromatic Cu-K α radiation in a scanning range of 4 and 40° using a scan step size of 8° min⁻¹.

Elemental analysis

Elemental analysis was performed by the Analysis Service of the Faculty of Chemistry of the University of Strasbourg.

EDS experiments

Elemental analyses using EDS were performed on a Bruker-QUANTAX System, where the EDS Detector was equipped with a GEMINI FE-SEM ULTRA55 (Carl Zeiss). The samples were mixed with colloidal graphite in isopropanol, dried and pressed into pellets. The EDS analysis was conducted at an accelerating voltage of 15 kV.

Photophysical properties

Luminescence and excitation spectra were recorded on a Fluorolog 3-22 (Horiba Jobin Yvon).

The absolute luminescence quantum yields and luminescence lifetimes were determined using an absolute luminescence quantum yield spectrometer C9920-02 (Hamamatsu Photonics K. K.) and a Quantaurus-Tau C11367-12 (Hamamatsu Photonics K. K.), respectively, with pulsed excitation light sources.



Magnetic properties

The magnetic properties were investigated using a Quantum Design MPMS-3 Evercool magnetometer with the powder sample of **HL3-Dy** dispersed in paraffin oil to avoid the rotation of the crystals under the magnetic field. The magnetic data were corrected for the diamagnetic contributions from the sample, oil and the sample holder.

Synthesis

All reagents were purchased from commercial sources and used without further purification. **H₄L3** was prepared using a previously reported procedure with some modifications.^{63,74}

Crystallization conditions

HL3-Tb. A solution containing **H₄L3** (5 mg, 0.005 mmol) dissolved in DMF (1 mL) was mixed with a 0.01 M solution of $\text{Tb}(\text{NO}_3)_3 \cdot 6\text{H}_2\text{O}$ in DMF (1 mL, 0.01 mmol). Then, 2 drops of 1 M HCl were added to the mixture. In a vial closed with a cap, the solution was heated at 80 °C for 3 days, and after cooling to RT, colourless single crystals were obtained (5.3 mg, 73%). They were filtrated and washed with DMF (2 mL) and diethyl ether (2 mL). Formula: $\text{C}_{60}\text{H}_{81}\text{TbN}_4\text{O}_{16}\text{S}_4$, anal. calcd: C, 51.42%; H, 5.83%; N, 4.00%; found: C, 51.45%; H, 5.87%; N, 4.06%.

HL3-Tb_{0.95}Dy_{0.05}. The same procedure was applied starting from a 0.01 M solution of $\text{Tb}(\text{NO}_3)_3 \cdot 6\text{H}_2\text{O}$ in DMF (0.95 mL, 0.0095 mmol) and a 0.01 M solution of $\text{Dy}(\text{NO}_3)_3 \cdot 5\text{H}_2\text{O}$ (0.05 mL, 0.005 mmol). Yield, 4.6 mg (64%). Formula: $\text{C}_{60}\text{H}_{81}\text{Tb}_{0.05}\text{Dy}_{0.95}\text{N}_4\text{O}_{16}\text{S}_4$, anal. calcd: C, 51.30%; H, 5.81%; N, 3.99%; found: C, 51.38%; H, 5.85%; N, 4.05%.

HL3-Tb_{0.67}Dy_{0.33}. The same procedure was applied starting from a 0.01 M solution of $\text{Tb}(\text{NO}_3)_3 \cdot 6\text{H}_2\text{O}$ in DMF (0.75 mL, 0.0075 mmol) and a 0.01 M solution of $\text{Dy}(\text{NO}_3)_3 \cdot 5\text{H}_2\text{O}$ (0.25 mL, 0.0025 mmol). Yield, 4.5 mg (62%). Formula: $\text{C}_{60}\text{H}_{81}\text{Tb}_{0.67}\text{Dy}_{0.33}\text{N}_4\text{O}_{16}\text{S}_4$, anal. calcd: C, 51.38%; H, 5.82%; N, 4.00%; found: C, 51.42%; H, 5.96%; N, 4.08%.

HL3-Tb_{0.42}Dy_{0.58}. The same procedure was applied starting from a 0.01 M solution of $\text{Tb}(\text{NO}_3)_3 \cdot 6\text{H}_2\text{O}$ in DMF (0.5 mL, 0.005 mmol) and a 0.01 M solution of $\text{Dy}(\text{NO}_3)_3 \cdot 5\text{H}_2\text{O}$ (0.5 mL, 0.005 mmol). Yield, 5.2 mg (65%). Formula: $\text{C}_{60}\text{H}_{81}\text{Tb}_{0.42}\text{Dy}_{0.58}\text{N}_4\text{O}_{16}\text{S}_4$, anal. calcd: C, 51.35%; H, 5.82%; N, 3.99%; found: C, 51.52%; H, 5.85%; N, 3.98%.

HL3-Tb_{0.2}Dy_{0.8}. The same procedure was applied starting from a 0.01 M solution of $\text{Tb}(\text{NO}_3)_3 \cdot 6\text{H}_2\text{O}$ in DMF (0.25 mL, 0.0025 mmol) and a 0.01 M solution of $\text{Dy}(\text{NO}_3)_3 \cdot 5\text{H}_2\text{O}$ (0.75 mL, 0.0075 mmol). Yield, 5.8 mg (75%). Formula: $\text{C}_{60}\text{H}_{81}\text{Tb}_{0.2}\text{Dy}_{0.8}\text{N}_4\text{O}_{16}\text{S}_4$, anal. calcd: C, 51.32%; H, 5.81%; N, 3.99%; found: C, 51.39%; H, 5.83%; N, 4.02%.

HL3-Tb_{0.07}Dy_{0.93}. The same procedure was applied starting from a 0.01 M solution of $\text{Tb}(\text{NO}_3)_3 \cdot 6\text{H}_2\text{O}$ in DMF (0.1 mL, 0.001 mmol) and a 0.01 M solution of $\text{Dy}(\text{NO}_3)_3 \cdot 5\text{H}_2\text{O}$ (0.9 mL, 0.009 mmol). Yield, 5.3 mg (73%). Formula: $\text{C}_{60}\text{H}_{81}\text{Tb}_{0.07}\text{Dy}_{0.93}\text{N}_4\text{O}_{16}\text{S}_4$, anal. calcd: C, 51.30%; H, 5.81%; N, 3.99%; found: C, 51.45%; H, 5.79%; N, 4.08%.

HL3-Dy. The same procedure was applied starting from a 0.01 M solution of $\text{Dy}(\text{NO}_3)_3 \cdot 5\text{H}_2\text{O}$ in DMF (1 mL, 0.01 mmol).

Yield, 4.8 mg (68%). Formula: $\text{C}_{60}\text{H}_{81}\text{O}_{16}\text{N}_4\text{S}_4\text{Dy}$, anal. calcd: C, 51.29%; H, 5.81%; N, 3.99%; found: C, 51.35%; H, 5.86%; N, 4.02%.

Conflicts of interest

There are no conflicts to declare.

Acknowledgements

We thank the Russian Science Foundation (grant no. 17-73-20117) for financial support for the synthesis and crystal preparation. Financial supports from the University of Strasbourg, the International Centre for Frontier Research in Chemistry (icFRC), Laboratory of excellence LabEx CSC, Strasbourg, the Institut Universitaire de France, the CNRS, and MEXT Grants-in-Aid for Scientific Research on Innovative Areas of "Soft Crystals (Area Number: 2903, No. 17H06374) are acknowledged. Center for Instrumental Analysis, College of Science and Engineering, Aoyama Gakuin University also supports to analyse EDS.

Notes and references

- 1 B. F. Abrahams, B. F. Hoskins and R. Robson, A new type of infinite 3D polymeric network containing 4-connected, peripherally-linked metalloporphyrin building blocks, *J. Am. Chem. Soc.*, 1991, **113**, 3606–3607.
- 2 S. R. Batten and R. Robson, Interpenetrating Nets: Ordered, Periodic Entanglement, *Angew. Chem., Int. Ed.*, 1998, **37**, 1460–1494.
- 3 Special issue on Metal–Organic Frameworks: *Chem. Rev.*, 2012, **112**.
- 4 M. W. Hosseini, Reflexion on molecular tectonics, *CrystEngComm*, 2004, **6**, 318–322.
- 5 M. W. Hosseini, Molecular Tectonics: From Simple Tectons to Complex Molecular Networks, *Acc. Chem. Res.*, 2005, **38**, 313–323.
- 6 G. Férey, C. Serre, T. Devic, G. Maurin, H. Jobic, P. L. Llewellyn, G. De Weireld, A. Vimont, M. Daturi and J.-S. Chang, Why hybrid porous solids capture greenhouse gases?, *Chem. Soc. Rev.*, 2011, **40**, 550–562.
- 7 H.-C. Zhou, J. R. Long and O. M. Yaghi, Introduction to Metal–Organic Frameworks, *Chem. Rev.*, 2012, **112**, 673–674.
- 8 L. Q. Ma, C. Abney and W. B. Lin, Enantioselective catalysis with homochiral metal–organic frameworks, *Chem. Soc. Rev.*, 2009, **38**, 1248–1256.
- 9 M. Yoon, R. Srirambalaji and K. Kim, Homochiral Metal–Organic Frameworks for Asymmetric Heterogeneous Catalysis, *Chem. Rev.*, 2012, **112**, 1196–1231.
- 10 P. Dechambenoit and J. R. Long, Microporous magnets, *Chem. Soc. Rev.*, 2011, **40**, 3249–3265.
- 11 G. M. Espallargas and E. Coronado, Magnetic functionalities in MOFs: from the framework to the pore, *Chem. Soc. Rev.*, 2018, **47**, 533–557.

12 M. D. Allendorf, C. A. Bauer, R. K. Bhakta and R. J. T. Houk, Luminescent metal-organic frameworks, *Chem. Soc. Rev.*, 2009, **38**, 1330–1352.

13 B. Chen, S. Xiang and G. Qian, Metal-Organic Frameworks with Functional Pores for Recognition of Small Molecules, *Acc. Chem. Res.*, 2010, **43**, 1115–1124.

14 Y. Cui, Y. Yue, G. Qian and B. Chen, Luminescent Functional Metal-Organic Frameworks, *Chem. Rev.*, 2012, **112**, 1126–1162.

15 *Advances in Inorganic chemistry, Supramolecular Chemistry*, ed. R. van Eldik and R. Puchta, Academic Press, 2018.

16 J. Rocha, L. D. Carlos, F. A. A. Paz and D. Ananias, Luminescent multifunctional lanthanides-based metal-organic frameworks, *Chem. Soc. Rev.*, 2011, **40**, 926–940.

17 Y. Cui, B. Chen and G. Qian, Lanthanide metal-organic frameworks for luminescent sensing and light-emitting applications, *Coord. Chem. Rev.*, 2014, **273–274**, 76–86.

18 Y. Cui, B. Li, H. He, W. Zhou, B. Chen and G. Qian, Metal-Organic Frameworks as Platforms for Functional Materials, *Acc. Chem. Res.*, 2016, **49**, 483–493.

19 S. Roy, A. Chakraborty and T. K. Maji Qian, Lanthanide-organic frameworks for gas storage and as magneto-luminescent materials, *Coord. Chem. Rev.*, 2014, **273–274**, 139.

20 Y. Hasegawa and T. Nakanishi, Luminescent lanthanide coordination polymers for photonic applications, *RSC Adv.*, 2015, **5**, 338–353.

21 J. Wu, H. Zhang and S. Du, Tunable luminescence and white light emission of mixed lanthanide-organic frameworks based on polycarboxylate ligands, *J. Mater. Chem. C*, 2016, **1**, 3364–3374.

22 S. Tobita, M. Arakawa and I. Tanaka, The paramagnetic metal effect on the ligand localized S1~T1 intersystem crossing in the rare-earth-metal complexes with methyl salicylate, *J. Phys. Chem.*, 1985, **89**, 5649–5654.

23 J. C. G. Bünzli, Review: Lanthanide coordination chemistry: from old concepts to coordination polymers, *J. Coord. Chem.*, 2014, **67**, 3706–3733.

24 Q. Zha, X. Rui, T. Wei and Y. Xie, Recent advances in the design strategies for porphyrin-based coordination polymers, *CrystEngComm*, 2014, **16**, 7371–7384.

25 J. J. Baldovi, E. Coronado, A. Gaita-Arino, C. Gamer, M. Gimenez-Marques and G. Minguez Espallargas, A Sim-MOF: Three-Dimensional Organisation of Single-Ion Magnets with Anion-Exchange Capabilities, *Chem.-Eur. J.*, 2014, **20**, 10695–10702.

26 X. Zhang, V. Vieru, X. Feng, J.-L. Liu, Z. Zhang, B. Na, W. Shi, B.-W. Wang, A. K. Powell, L. F. Chibotaru, S. Gao, P. Cheng and J. R. Long, Influence of Guest Exchange on the Magnetization Dynamics of Dilanthanide Single-Molecule-Magnet Nodes within a Metal-Organic Framework, *Angew. Chem., Int. Ed.*, 2015, **54**, 9861–9865.

27 D.-D. Yin, Q. Chen, Y.-S. Meng, H.-L. Sun, Y.-Q. Zhang and S. Gao, Slow magnetic relaxation in a novel carboxylate/oxalate/hydroxyl bridged dysprosium layer, *Chem. Sci.*, 2015, **6**, 3095–3101.

28 S. Mohapatra, B. Rajeswaran, A. Chakraborty, A. Sundaresan and T. K. Maji, Bimodal Magneto-Luminescent Dysprosium (DyIII)-Potassium (K) Oxalate Framework: Magnetic Switchability with High Anisotropic Barrier and Solvent Sensing, *Chem. Mater.*, 2013, **25**, 1673–1679.

29 R. Jankowski, J. J. Zakrzewski, O. Surma, S. Ohkoshi, S. Chorazy and B. Sieklucka, Near-infrared emissive Er(III) and Yb(III) molecular nanomagnets in metal-organic chains functionalized by octacyanidometallates(IV), *Inorg. Chem. Front.*, 2019, **6**, 2423–2434.

30 Y. Xin, J. Wang, M. Zychowicz, J. J. Zakrzewski, K. Nakabayashi, B. Sieklucka, S. Chorazy and S. Ohkoshi, Dehydration–Hydration Switching of Single-Molecule Magnet Behavior and Visible Photoluminescence in a Cyanido-Bridged DyIII/CoIII Framework, *J. Am. Chem. Soc.*, 2019, **141**, 18211–18220.

31 C. D. Gutsche in *Calixarenes Revised: Monographs in Supramolecular Chemistry*, The Royal Society of Chemistry, Cambridge, 1998, vol. 6.

32 Z. Asfari, V. Böhmer, J. Harrowfield and J. Vicens, in *Calixarenes 2001*, ed. Z. Asfari, V. Böhmer, J. Harrowfield and J. Vicens, Kluwer Academic, Dordrecht, 2001.

33 M. W. Hosseini, *ACS Series*, ed. G. J. Lumetta, R. D. Rogers and A. S. Gopalan, 2000, vol. 557, p. 296.

34 H. Kumagai, M. Hasegawa, S. Miyanari, Y. Sugawa, Y. Sato, T. Hori, S. Ueda, H. Kamiyama and S. Miyano, Facile synthesis of *p*-tert-butylthiacalix[4]arene by the reaction of *p*-tert-butylphenol with elemental sulfur in the presence of a base, *Tetrahedron Lett.*, 1997, **38**, 3971–3972.

35 P. Rao, M. W. Hosseini, A. De Cian and J. Fischer, Synthesis and structural analysis of mercaptothiacalix[4]arene, *Chem. Commun.*, 1999, 2169–2170.

36 H. Akdas, E. Graf, M. W. Hosseini, A. de Cian, A. Bilyk, B. W. Skelton, G. A. Koutsantonis, I. Murray, J. M. Harrowfield and A. H. White, Koilands from thiophiles: mercury(II) clusters from thiocalixarenes, *Chem. Commun.*, 2002, 1042–1043.

37 A. Ovsyannikov, S. Solovieva, I. Antipin and S. Ferlay, Coordination Polymers based on calixarene derivatives: Structures and properties, *Coord. Chem. Rev.*, 2017, **352**, 151–186.

38 F. M. Ramirez, L. Charbonnière, G. Muller and J.-C. G. Bünzli, Tuning the Stoichiometry of Lanthanide Complexes with Calixarenes: Bimetallic Complexes with a Calix[6]arene Bearing Ether-Amide Pendant Arms, *Eur. J. Inorg. Chem.*, 2004, 2348–2355.

39 K. Z. Su, F. L. Jiang, J. J. Qian, J. D. Pang, F. L. Hu, S. M. Bawaked, M. Mokhtar, S. A. Al-Thabaiti and M. Hong, Synthesis and characterization of decanuclear Ln(III) cluster of mixed calix[8]arene-phosphonate ligands (Ln = Pr, Nd), *Inorg. Chem. Commun.*, 2015, **54**, 34–37.

40 T. Kajiwara, N. Iki and M. Yamashita, Transition metal and lanthanide cluster complexes constructed with thiocalix[n] arene and its derivatives, *Coord. Chem. Rev.*, 2007, **251**, 1734–1746.

41 B. S. Creavena, D. F. Donlon and J. McGinley, Coordination chemistry of calix[4]arene derivatives with lower rim



functionalisation and their applications, *Coord. Chem. Rev.*, 2009, **253**, 893–962.

42 S. Sanz, R. D. McIntosh, C. M. Beavers, S. J. Teat, M. Evangelisti, E. K. Brechin and S. J. Dalgarno, Calix[4]arene-supported rare earth octahedra, *Chem. Commun.*, 2012, **48**, 1449–1451.

43 J. P. Chinta, B. Ramanujam and C. P. Rao, Structural aspects of the metal ion complexes of the conjugates of calix[4]arene: Crystal structures and computational models, *Coord. Chem. Rev.*, 2012, **256**, 2762–2794.

44 Y. F. Bi, Y. L. Li, W. P. Liao, H. J. Zhang and D. Q. Li, A Unique Mn_2Gd_2 Tetranuclear Compound of *p*-*tert*-Butylthiocalix[4]arene, *Inorg. Chem.*, 2008, **47**, 9733–9734.

45 Y. F. Bi, X. T. Wang, B. W. Wang, W. P. Liao, X. F. Wang, H. J. Zhang, S. Gao and D. Q. Li, Two $MnII_2LnIII_4$ ($Ln = Gd, Eu$) hexanuclear compounds of *p*-*tert*-butylsulfinylcalix[4]arene, *Dalton Trans.*, 2009, **12**, 2250–2254.

46 G. Karotsis, S. Kennedy, S. J. Teat, C. M. Beavers, D. A. Fowler, J. J. Morales, M. Evangelisti, S. J. Dalgarno and E. K. Brechin, $[MnIII_4LnIII_4]$ Calix[4]arene Clusters as Enhanced Magnetic Coolers and Molecular Magnets, *J. Am. Chem. Soc.*, 2010, **132**, 12983–12990.

47 S. Sanz, K. Ferreira, R. D. McIntosh, S. J. Dalgarno and E. K. Brechin, Calix[4]arene-supported $Fe^{III}_2Ln^{III}_2$ clusters, *Chem. Commun.*, 2011, **47**, 9042–9044.

48 Y. Bi, S. Du and W. Liao, Thiocalixarene-based nanoscale polyhedral coordination cages, *Coord. Chem. Rev.*, 2014, **276**, 61–72.

49 M. Coletta, R. McLellan, A. Waddington, S. Sanz, K. J. Gagnon, S. J. Teat, E. K. Brechin and S. J. Dalgarno, Core expansion of bis-calix[4]arene-supported clusters, *Chem. Commun.*, 2016, **52**, 14246–14249.

50 M. Coletta, R. McLellan, S. Sanz, K. J. Gagnon, S. J. Teat, E. K. Brechin and S. J. Dalgarno, A New Family of 3d-4f Bis-Calix[4]arene-Supported Clusters, *Chem.-Eur. J.*, 2017, **23**, 14073–14079.

51 H. Han, X. Li, X. Zhu, G. Zhang, S. Wang, X. Hang, J. Tang and W. Liao, Single-Molecule-Magnet Behavior in a Calix[8]arene-Capped $\{Tb_6III_6CrIII\}$ Cluster, *Eur. J. Inorg. Chem.*, 2017, 2088–2093.

52 A. Jäschke, M. Kischel, A. Mansel and B. Kersting, Hydroxyquinoline-Calix[4]arene Conjugates as Ligands for Polynuclear Lanthanide Complexes: Preparation, Characterization, and Properties of a Dinuclear EuIII Complex, *Eur. J. Inorg. Chem.*, 2017, 894–901.

53 R. S. Viana, C. A. F. Oliveira, J. Chojnacki, B. S. Barros, S. Alves Jr and J. Kulesza, Structural and spectroscopic investigation of new luminescent hybrid materials based on calix[4]arene-tetracarboxylate and Ln^{3+} ions ($Ln = Gd, Tb$ or Eu), *J. Solid State Chem.*, 2017, **251**, 26–32.

54 S. J. Dalgarno, M. J. Hardie, J. L. Atwood and C. L. Raston, Bilayers, Corrugated Bilayers, and Coordination Polymers of *p*-Sulfonatocalix[6]arene, *Inorg. Chem.*, 2004, **43**, 6351–6356.

55 W. Liao, C. Liu, X. Wang, G. Zhu, X. Zhao and H. Zhang, 3D metal-organic frameworks incorporating water-soluble tetra-*p*-sulfonatocalix[4]arene, *CrystEngComm*, 2009, **11**, 2282–2284.

56 I. Ling, Y. Alias and C. L. Raston, Structural diversity of multi-component self-assembled systems incorporating *p*-sulfonatocalix[4]arene, *New J. Chem.*, 2010, **34**, 1802–1811.

57 I. Ling and C. L. Raston, Primary and secondary directing interactions of aquated lanthanide(III) ions with *p*-sulfonated calix[n]arene, *Coord. Chem. Rev.*, 2018, **375**, 80–105.

58 K. Kim, S. Park, K.-M. Park, K.-M. Park and S. S. Lee, Thiocalix[4]arene-Based Three-Dimensional Coordination Polymers Incorporating Neutral Bridging Coligands, *Cryst. Growth Des.*, 2011, **11**, 4059–4067.

59 Z. Zhang, A. Drapailo, Y. Matvieiev, L. Wojtas and M. J. Zaworotko, A calixarene based metal organic material, calixMOM, that binds potassium cations, *Chem. Commun.*, 2013, 8353–8355.

60 H. Akdas, E. Graf, M. W. Hosseini, A. De Cian and J. McB. Harrowfield, Design, synthesis and structural investigation of a 2-D coordination network based on the self-assembly of the tetracarboxylate derivative of tetrathiocalix[4]arene, *Commun.*, 2000, 2219–2220.

61 J.-Y. Kim, K. Kim, K.-M. Park and S. S. Lee, Isostructural Heteronuclear (K^+/M^{2+} : $M = Ni, Co$, and Zn) One-Dimensional Coordination Polymers of Thiocalix[4]arene Tetraacetate, *Bull. Korean Chem. Soc.*, 2014, **35**, 289–292.

62 A. S. Ovsyannikov, S. Ferlay, S. E. Solovieva, I. S. Antipin, A. I. Konovalov, N. Kyritsakas and M. W. Hosseini, Molecular tectonics: high dimensional coordination networks based on methylenecarboxylate-appended tetramercaptothiocalix[4]arene in the 1,3-alternate conformation, *CrystEngComm*, 2018, **20**, 1130–1140.

63 A. S. Ovsyannikov, M. Lang, S. Ferlay, S. E. Solovieva, I. S. Antipin, A. I. Konovalov, N. Kyritsakas and M. W. Hosseini, Molecular tectonics: tetracarboxythiocalix[4]arene derivatives as tectons for the formation of hydrogen-bonded networks, *CrystEngComm*, 2016, **18**, 8622–8630.

64 K. A. White, D. A. Chengelis, K. A. Gogick, J. Stehman, N. L. Rosi and S. Petoud, Near-Infrared Luminescent Lanthanide MOF Barcodes, *J. Am. Chem. Soc.*, 2009, **131**, 18069–18071.

65 S. Dang, J. H. Zhang and Z. M. Sun, Tunable emission based on lanthanide(III) metal-organic frameworks: an alternative approach to white light, *J. Mater. Chem.*, 2012, **22**, 8868–8873.

66 V. Haquin, M. Etienne, C. Daiguebonne, S. Freslon, G. Calvez, K. Bernot, L. Le Pollès, S. E. Ashbrook, M. R. Mitchell, J.-C. Bünzli, S. V. Eliseeva and O. Guillou, Color and Brightness Tuning in Heteronuclear Lanthanide Terephthalate Coordination Polymers, *Eur. J. Inorg. Chem.*, 2013, 3464–3476.

67 D. T. de Lill, N. S. Gunning and C. L. Cahill, Toward Templated Metal-Organic Frameworks: Synthesis, Structures, Thermal Properties, and Luminescence of Three Novel Lanthanide-Adipate Frameworks, *Inorg. Chem.*, 2005, **44**, 258–266.



68 K. Liu, H. You, Y. Zheng, G. Jia, Y. Song, Y. Huang, M. Yang, J. Jia, N. Guo and H. Zhang, Facile and rapid fabrication of metal-organic framework nanobelts and color-tunable photoluminescence properties, *J. Mater. Chem.*, 2010, **20**, 3272–3279.

69 S. Mohapatra, S. Adhikari, H. Riju and T. K. Maji, Terbium(III), Europium(III), and Mixed Terbium(III)-Europium(III) Mucic acid Frameworks: Hydrophilicity and Stoichiometry-Dependent Color Tunability, *Inorg. Chem.*, 2012, **51**, 4891–4893.

70 Y. Cui, H. Xu, Y. Yue, Z. Guo, J. Yu, Z. Chen, J. Gao, Y. Yang, G. Qian and B. Chen, A Luminescent Mixed-Lanthanide Metal-Organic Framework Thermometer, *J. Am. Chem. Soc.*, 2012, **134**, 3979–3982.

71 A. R. Ramya, D. Sharma, S. Natarajan and M. L. P. Reddy, Highly Luminescent and Thermally Stable Lanthanide Coordination Polymers Designed from 4-(Dipyridin-2-yl) aminobenzoate: Efficient Energy Transfer from Tb³⁺ to Eu³⁺ in a Mixed Lanthanide Coordination Compound, *Inorg. Chem.*, 2012, **51**, 8818–8826.

72 S. Sato, A. Ishii, C. Yamada, J. Kim, H. S. Chul, A. Fujiwara, M. Takata and M. Hasegawa, Luminescence of fusion materials of polymeric chain-structured lanthanide complexes, *Polym. J.*, 2015, **47**, 195–200.

73 K. Kumar, S. Chorazy, K. Nakabayashi, H. Sato, B. Sieklucka and S.-I. Ohkoshi, TbCo and Tb_{0.5}Dy_{0.5}Co layered cyanido-bridged frameworks for construction of colorimetric and ratiometric luminescent thermometers, *J. Mater. Chem. C*, 2018, **6**, 8372–8384.

74 H. Akdas, G. Mislin, E. Graf, M. Hosseini, A. De Cian and J. Fisher, Synthesis and solid state structural analysis of conformers of tetrakis[(ethoxycarbonyl)methoxy]tetrathiocalix[4]arene, *Tetrahedron Lett.*, 1999, **40**, 2113–2116.

75 N. Iki, N. Morohashi, F. Narumi, T. Fujimoto, T. Suzuki and S. Miyano, Novel molecular receptors based on a thiocalix[4]arene platform. Preparations of the di- and tetracarboxylic acid derivatives and their binding properties towards transition metal ions, *Tetrahedron Lett.*, 1999, **40**, 7337–7341.

76 The program is available free of charge at <http://www.ee.ub.edu/>.

77 G. F. de Sá, O. L. Malta, C. M. Donegá, A. M. Simas, R. L. Longo, P. A. Santa-Cruz and E. F. da Silva Jr, Spectroscopic properties and design of highly luminescent lanthanide coordination complexes, *Coord. Chem. Rev.*, 2000, **196**, 165–195.

78 M. F. Hazenkamp, G. Blasse, N. Sabbatini and R. Ungaro, The solid state luminescence of the encapsulation complex of Eu³⁺ in *p*-*t*-butyl-calix[4]arene tetra-amide, *Inorg. Chim. Acta*, 1990, **172**, 93–95.

79 D. Woodruff, R. E. P. Winpenny and R. A. Layfield, Lanthanide Single-Molecule Magnets, *Chem. Rev.*, 2013, **113**, 5110–5148.

80 Y.-N. Guo, G.-F. Xu, Y. Guo and J. Tang, Relaxation dynamics of dysprosium(III) single molecule magnets, *Dalton Trans.*, 2011, **40**, 9953–9963.

81 A. Amjad, A. Figuerola and L. Sorace, Tm(III) complexes undergoing slow relaxation of magnetization: exchange coupling and aging effects, *Dalton Trans.*, 2017, **46**, 3848–3856.

82 K. S. Pedersen, J. Dreiser, H. Weihe, R. Sibile, H. V. Johannessen, M. A. Sorensen, B. E. Nielsen, M. Sigrist, H. Mutka, S. Rols, J. Bendix and S. Piligkos, Design of Single-Molecule Magnets: Insufficiency of the Anisotropy Barrier as the Sole Criterion, *Inorg. Chem.*, 2015, **54**, 7600–7606.

83 S. Chorazy, J. J. Zakrzewski, M. Reczyński, K. Nakabayashi, S. Ohkoshi and B. Sieklucka, Humidity driven molecular switch based on photoluminescent Dy³⁺Co³⁺ single-molecule magnets, *J. Mater. Chem. C*, 2019, **7**, 4164–4172.

84 J. J. Zakrzewski, S. Chorazy, K. Nakabayashi, S. Ohkoshi and B. Sieklucka, Photoluminescent Lanthanide(III) Single-Molecule Magnets in Three-Dimensional Polycyanidocuprate(I)-Based Frameworks, *Chem.-Eur. J.*, 2019, **25**, 11820–11825.

85 J.-H. Jia, Q.-W. Li, Y.-C. Chen, J.-L. Liu and M.-L. Tong, Luminescent single-molecule magnets based on lanthanides: Design strategies, recent advances and magneto-luminescent studies, *Coord. Chem. Rev.*, 2019, **378**, 365–381.

86 G. M. Sheldrick, A short history of SHELX, *Acta Crystallogr., Sect. A: Found. Crystallogr.*, 2008, **64**, 112–122.

